Nanodroplet Activated and Guided Folding of Graphene Nanostructures

Niladri Patra, Boyang Wang, and Petr Král*

Department of Chemistry, University of Illinois at Chicago, Chicago, Illinois 60607, USA

ABSTRACT

We demonstrate by molecular dynamics simulations that water nanodroplets can activate and guide the folding of planar graphene nanostructures. Once the nanodroplets are deposited at selected spots on the planar nanostructure, they can act as catalytic elements that initiate conformational changes and help to overcome deformation barriers associated with them. Nanodroplets can induce rapid bending, folding, sliding, rolling, and zipping of the planar nanostructures, which can lead to the assembly of nanoscale sandwiches, capsules, knots, and rings.

The essence of "bottom-up" material preparation techniques is to guide the self-assembly of material units toward the final structures.[1,2] Although they can be far less energy and material demanding than the popular "top-down" techniques, their use is mostly limited to biomineralization and other biologically guided processes.[3] In order to overcome the lack of guidance at the nanoscale, we might receive help from biological systems, as recently shown by Belcher on the preparation of battery electrodes by viruses.[4] Alternatively, we need to learn how to precisely control the competition of van der Waals (vdW), Coulombic, entropic, and other forces,[5] in order to tailor precisely ordered structures. Once mastered, the guided assembly processes should allow reproducible preparation of complex structures, such as nanoparticles[6−9] and nanorod[10,11] superlattices.

Recently, graphene monolayers have been prepared and intensively studied.[12−15] Graphene nanoribbons have also been synthesized,[16−18] and etched by using lithography[19,20] and catalytic[21,22] methods. *Graphene flakes* with strong interlayer vdW binding can self-assemble into larger structures.[23−25] Individual flakes with high elasticity[26−28] could also fold into a variety of 3D structures, such as carbon nanoscrolls.[29,30] These nanoscrolls could be even prepared from single graphene sheets, when assisted by certain gases or alcohols.[31,32] In order to reproducibly prepare such stable or metastable structures of different complexity, (1) the potential barriers associated with graphene deformation need to be overcome, (2) the folding processes should be guided, and (3) the final structures need to be well coordinated and stabilized by vdW or other coupling mechanisms.

Carbon nanotubes (CNTs) can serve as a railroad for small water droplets.[33] CNTs submerged in water can assemble into microrings around bubbles formed by ultrasonic waves.[34]
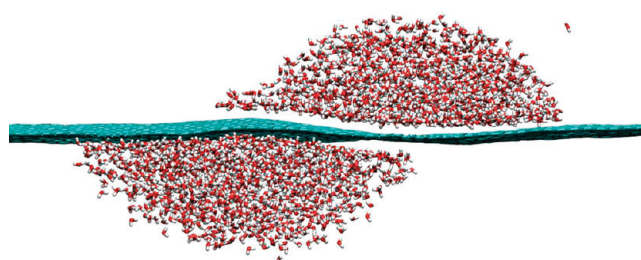

Figure 1. Side view on two water nanodroplets, each with $N_w = 1300$ molecules, adsorbed on the opposite sides of a graphene sheet. The nanodroplets create two shallow holes in the graphene. Eventually, the nanodroplets become adjacent but stay highly mobile. Their dynamical coupling is realized by the minimization of the graphene bending energy associated with the two holes.

Similar assembly effects might work in 2D graphene-based systems. For example, liquid droplets can induce wrinkles on thin polymer films by strong capillary forces.[35] Droplets can also guide folding of 3D microstructures from polymer (PDMS) sheets.[36] *The question is if nanodroplets (NDs) can activate and guide folding of graphene flakes of complex shapes, analogously like chaperones fold proteins.*[37] To answer this question, we study first the interaction of a water nanodroplet, of $N_w = 1300$ waters, with a graphene sheet, of the size of 15×12 nm^2. We model this system by molecular dynamics (MD) simulations with the NAMD package with CHARMM27 force field.[38−40] It turns out that the nanodroplet, equilibrated at $T = 300$ K, induces a shallow hole in the graphene sheet, with the curvature radius of $R \approx 5$ nm. The hole formation is driven by vdW coupling, which tends to minimize the surface of the naked droplet but maximize the surface of the graphene-dressed droplet. As shown in Figure 1, two such droplets adsorbed on the opposite sides of the graphene sheet couple to save on the
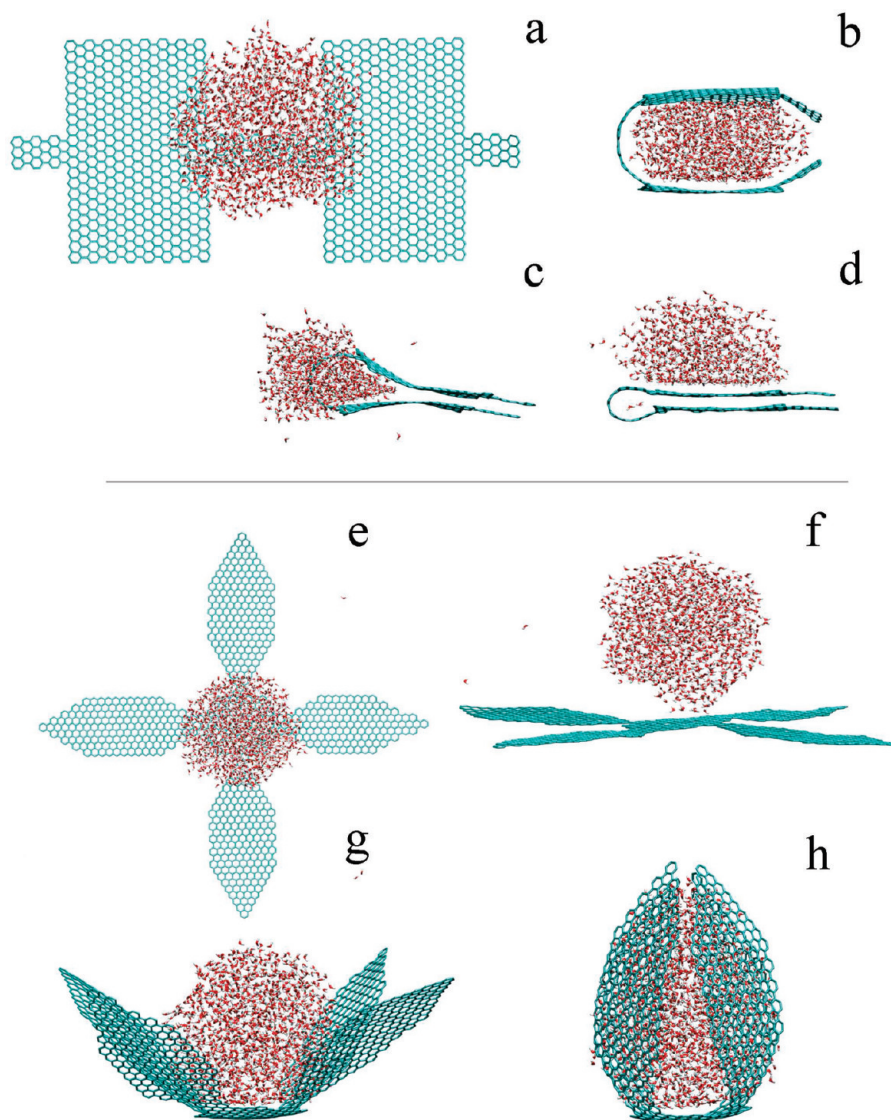
* Corresponding author, pkral@uic.edu.

Figure 2. (a–d) Water nanodroplet activated and guided folding of two graphene flakes connected by a narrow bridge. The nanodroplet is squeezed away when the system is heated to $T = 400$ K. (e–h) Nanodroplet-assisted folding of a star-shaped graphene flake, resembling the action of a "meat-eating flower"(see movie in Supporting Information).

hole formation energy. The two droplets stay together during a correlated diffusion motion on the graphene surface.

Folding of Flakes. Intrigued by the action of NDs on graphene, we test to see if they can activate and guide folding of graphene flakes of various shapes. As shown in Figure 2a, we first design a graphene nanoribbon, where two rectangular 3×5 nm^2 flakes are connected by a narrow stripe of 2.5×0.73 nm^2. In the simulations, we fix a few stripes of benzene rings on the right flake, which could be realized if the graphene is partly fixed at some substrate, and position a water nanodroplet ($N_w = 1300$) above the center of the two flakes ($T = 300$ K). (b) After $t \approx 250$ ps, both flakes bind with the droplet and bend the connecting bridge to form a metastable sandwich structure. (c) When the temperature is raised to $T = 400$ K, the droplet becomes more mobile and fluctuating. Within $t \approx 50$ ps, the two flakes start to bind each other, and the water droplet is squeezed away. (d) After another $t \approx 60$ ps, the flakes join each other into a double layer, and the droplet stays on the top of one flake.

When a smaller water droplet with $N_w = 800$ is placed on the nanoribbon, it induces its folding in a similar way and becomes squeezed out even faster (panels c and d).

Similarly, we study the folding of a star-shaped graphene nanoribbon with four blades connected to a central flake, as shown in Figure 2e,f. At $T = 300$ K, a water droplet ($N_w = 1300$) is initially positioned at the height of $h \approx 0.5$ nm above the central flake. (g) The droplet binds by vdW coupling with the central flake and induces bending of the four blades. (h) After $t \approx 1$ ns, the four blades fold into a closed structure, with waters filling its interior. This effect resembles the action of a "meat-eating flower",[41] where the graphene capsule can store and protect the liquid content in various environments. Notice that slight asymmetry of the flake does not change the character of the assembly process. In real systems, other molecules might also be adsorbed on the graphene flakes. Although these molecules are not considered here, they might coalesce with the water droplets and modify their properties in the assembly process. Experimentally, the droplets could

be deposited by Dip-Pen nanolithography[42] or atomic force microscopy.[43] This deposition can also cause side effects not considered here, such as passage additional momentum to the folding sheet.

In order to make sure that these results can be quantitatively matched to experiments, we calculate the flexural rigidity D of our graphene sheets and compare it with theoretical results.[44−46] We simulate a graphene sheet with the size of $a \times b = 3.7 \times 4.0$ nm^2, which is rolled on to a cylinder with the radius of $R = a/2\pi$; we use the CHARMM27 force field parameters $k_{bond} = 322.55$ kcal/mol/Å^2, $k_{angle} = 53.35$ kcal/(mol rad^2) and $k_{dihedral} = 3.15$ kcal/mol. From the simulations, we calculate the energy associated with the cylindrical deformation of the graphene sheet, to obtain its strain energy density σ_{ela}. This allows us to calculate the flexural rigidity D, by using the formula $\sigma_{ela} = (1/2)D\kappa^2$, where $\kappa = 1/R$ is valid in the linear elastic regime.[47] The obtained value of $D = 0.194$ nN nm (27.9 kcal/mol) is in close agreement with ab initio results, $D_1 = 0.238$ nN nm,[45] and other model studies, giving $D_2 = 0.11$ nN nm[46] and $D_3 = 0.225$ nN nm.[47] Therefore, our simulations should be reasonably close to potential experiments.

Folding of the two flakes into the sandwich, shown in Figure 2a,b, is driven by the decrease of the water−graphene binding energy, $E_{g-w} = -\sigma_{g-w}A_{g-w}$. Here, we estimate the density of the binding energy from our MD simulations[40] to be $\sigma_{g-w} \approx 20.8$ kcal/(mol nm^2). The water−graphene binding area of the narrow stripe (initial area) and the two flakes (final area) are $A_{g-w}^{ini} = 2.5 \times 0.7 = 1.75$ nm^2 and $A_{g-w}^{end} = 3 \times 5 \times (2) = 30$ nm^2, respectively. The elastic bending energy of the connecting stripe is $E_{ela} = \sigma_{ela}A_{ela}$, where $A_{ela} \approx A_{g-w}^{ini}$ is the bending area, and $\sigma_{ela} = (1/2)D\kappa^2$ is calculated for $D = 27.9$ kcal/mol and $\kappa = 1/R_g$, where R_g is the graphene ribbon radius. In this case, $R_g \approx 1$ nm, so $\sigma_{g-w} > \sigma_{ela} \approx 14$ kcal/(mol nm^2). This, together with $A_{g-w} \approx A_{ela}$, valid at the beginning of the folding process, means that $E_{g-w} + E_{ela} < 0$. During the folding process, the sandwich configuration becomes further stabilized, since E_{g-w} decreases by an order of magnitude, due to $A_{g-w} = A_{g-w}^{end}$.

The final squeezing of the nanodroplet out of the sandwich, shown in Figure 2c,d, means that graphene−graphene vdW binding is preferable to graphene−water vdW binding, for the force field parameters used in CHARMM27. Here, the (nonbonding) vdW coupling between i th and j th atoms is described by the Lennard-Jones potential

$$V_{i,j} = \varepsilon_{i,j}[(R_{min,i,j}/r_{i,j})^{12} - 2(R_{min,i,j}/r_{i,j})^6],$$
$$\varepsilon_{i,j} = \sqrt{\varepsilon_i\varepsilon_j}, \quad R_{min,i,j} = \frac{1}{2}(R_{min,i} + R_{min,j}) \tag{1}$$

where the parameters for graphene carbon are set to be $\varepsilon_C = -0.07$ kcal/mol, $R_{min,C} = 3.98$ Å, for water oxygen, $\varepsilon_O = -0.12$ kcal/mol, $R_{min,O} = 3.4$ Å, and for water hydrogen, $\varepsilon_H = -0.046$ kcal/mol, $R_{min,H} = 0.44$ Å.

Folding of Ribbons. We now test if NDs can induce folding of graphene nanoribbons. As shown in Figure 3a, we use a 30×2 nm^2 graphene nanoribbon, with one end fixed. At $T = 300$ K, a ND with $N_w = 1300$ water molecules
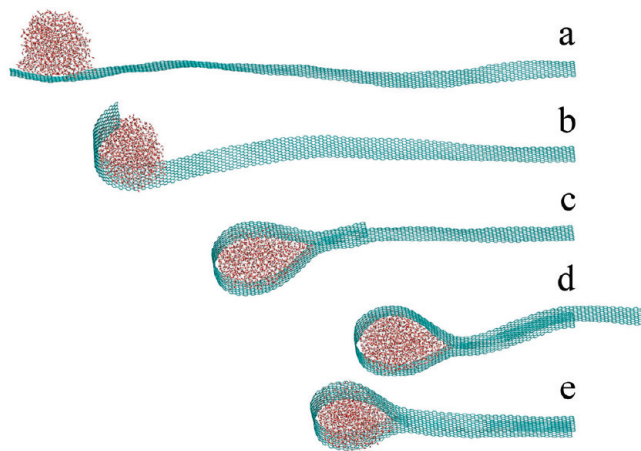

Figure 3. Folding and sliding of a graphene ribbon with the size of 30×2 nm, which is activated and guided by a nanodroplet with $N_w = 1300$ water molecules and the radius of $R_d \approx 2.1$ nm. (a−c) The free ribbon end folds around the droplet into a knot structure that slides on the ribbon surface (d, e)(see movie in Supporting Information).

is positioned above the free end of the ribbon. (b) The free end starts to fold fast around the droplet. (c) After $t = 0.6$ ns, the free end folds into a knot structure, touches the ribbon surface, and starts to slide fast on it, due to strong vdW binding. (d) While the knot is sliding on the ribbon, the droplet is deformed into a droplet-like shape that slips and rolls inside the knot.[33] After sliding over $l = 20$ nm, the water-filled knot gains the velocity of $v_w \approx 100$ m/s. This velocity is controlled by the rate of releasing potential energy, due to binding but reduced by bending, into the kinetic degrees of freedom, damped by friction. (d) The sliding ribbon reaches the fixed end and overstretches into the space, due to its large momentum. (e) It oscillates back and forth 2−3 times before the translational kinetic energy is dissipated.

The existence of CNTs raises the question if we could also "roll" graphene ribbons. This might happen when the droplet is larger and thus when it controls more the ribbon dynamics. In Figure 4a, we simulate the folding of a 90×2 nm^2 graphene ribbon (one end is fixed) at $T = 300$ K, when a droplet of $N_w = 10\,000$ is initially positioned above the tip of the ribbon. (b, c) As before, within $t = 2$ ps, the ribbon tip folds around the spherical droplet into a closed circular cylinder. (d) This time, the approaching free end touches the surface at a larger angle and forms a cylinder around the droplet that starts to roll fast on the ribbon surface, like a contracting tongue of a chameleon. After rolling over $l = 60$ nm, the translational and rolling velocities are $v_t \approx 50$ m/s and $\omega_r \approx 12$ rad/ns, respectively. (e) The cylinder rolls until the fixed end of the ribbon, where the rolling kinetic energy is eventually dissipated. The folded ribbon forms a multilayered ring structure, similar to multiwall nanotube, which is filled by water.

Let us analyze the conditions under which a graphene ribbon folds. Analogously to the folding of flakes, shown in Figure 2, the folding of ribbon is driven by the competition between the graphene−water binding energy, $E_{g-w} = $
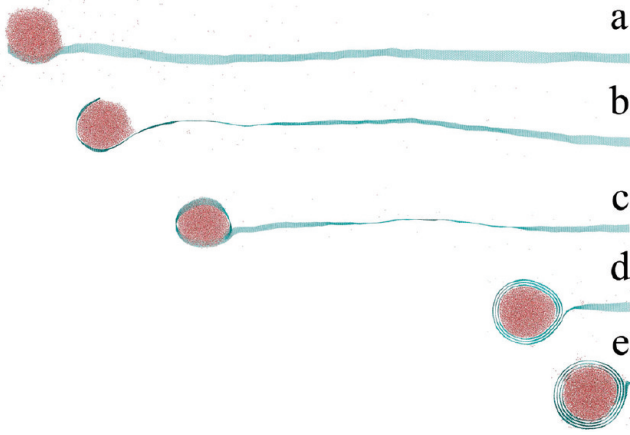
Figure 4. Folding and rolling of a graphene ribbon with the size of 90×2 nm, which is activated and guided by a nanodroplet with $N_w = 10000$ water molecules and the radius of $R_d \approx 4.2$ nm. (a, b) The ribbon tip folds around the water droplet into a wrapped cylinder, and (c−e) the wrapped cylinder is induced to roll on the ribbon surface (c−e) (see movie in Supporting Information).
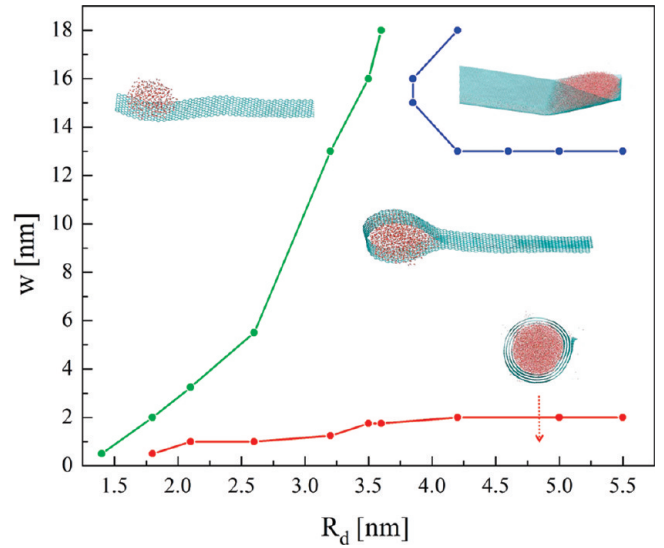

Figure 5. The phase diagram of a nanodroplet and graphene nanoribbon with different folding dynamics. We display the nonfolding, sliding, rolling, and zipping phases.

$-\sigma_{g\text{-}w}A_{g\text{-}w}$, and the graphene bending energy, $E_{ela} = \sigma_{ela}A_{ela}$. From the energy condition, $E_{g\text{-}w} + E_{ela} < 0$, we obtain

$$\frac{A_{g\text{-}w}}{A_{ela}} > \frac{\sigma_{ela}}{\sigma_{g\text{-}w}} \tag{2}$$

In Figure 3, the water droplet has the radius $R_d \approx 2.1$ nm. Assuming that $R_g \approx R_d$, we obtain from the above formula for σ_{ela} that $\sigma_{ela} = 3.2$ kcal/(mol nm^2) and $\sigma_{ela}/\sigma_{g\text{-}w} \approx 0.15$. Since, $A_{g\text{-}w}/A_{ela} \approx 1$, we see that this case easily fulfills the condition in eq 2. The graphene ribbon slides on itself, and this situation can be called the "sliding phase".

The ratio $A_{g\text{-}w}/A_{ela}$ and indirectly also σ_{ela} depend on the ratio of the ribbon width w to the droplet radius R_d, which thus controls the character of the folding process. When $w < 2R_d$, the droplet can bind, in principle, on the whole width of the ribbon, so $A_{g\text{-}w} \approx A_{ela}$. For even larger droplets, we eventually get $w < 0.5R_d$, where our simulations show that the ribbon binds fully to the droplet surface. In this limit, we observe that after folding once around the droplet circumference the ribbon approaches itself practically at the wetting angle and gains the dynamics characteristic for the "rolling phase", shown in Figure 4.

When $w > 2R_d$, it becomes very difficult for the small droplet to induce folding of the wide ribbon. Then the droplet binds to the ribbon at an approximately circular area, with a radius $\approx R_d$, because the water contact angle on graphene is about 90° and the droplet has almost the shape of a half-sphere.[48] If we assume that $R_g \approx R_d$, we have $A_{g\text{-}w} \approx \pi R_d^2$ and $A_{ela} \approx 2R_d w$. From eq 2 and $\sigma_{ela} = (1/2)D\kappa^2 = (1/2)D/R_d^2$, we then obtain the condition for the ribbon folding

$$R_d^3 > \frac{Dw}{\pi\sigma_{g\text{-}w}} \tag{3}$$

On the other hand, this means that the ribbon does not fold when $w \geq CR_d^3$ ($C = \pi\sigma_{g\text{-}w}/D \approx 4$ nm^{-2}), and this situation can be called the "nonfolding phase.

In Figure 5, we summarize the results of our simulations in a phase diagram. We display four "phases" characterizing the ribbon dynamics, separated by phase boundary lines. They are called nonfolding, sliding, rolling, and zipping, where the first three were described and briefly analyzed above. The nonfolding phase, where the ribbon end does not fold around the droplet, is characterized by the cubic boundary derived above and shown in Figure 5 (left). In the simulations, we obtain the value $C \approx 2.8$ nm^{-2}, in close agreement with the above prediction. The nonfolding phase is adjacent with the sliding phase, which is separated from the rolling phase by the boundary line $w \approx (1/2)R_d$.

When the graphene ribbon becomes several times wider than the droplet diameter, it may fold around it in the orthogonal direction. Then, the folding dynamics of the graphene ribbon has a character of zipping. This situation corresponds to the "zipping phase", shown in the right top corner of the phase diagram in Figure 5 and explained in detail in Figure 6. (a) We place a droplet of $N_w = 17000$ at the free end of the ribbon of the size of 60×16 nm^2. (b) The ribbon folds from the two sides of the droplet within $t \approx 250$ ps. (c) At $t \approx 450$ ps, the ribbon starts to "zip", where its two sides touch each other. (d) The zipping process continues, and the droplet is transported along the ribbon. After zipping over $l \approx 40$ nm, the droplet gains a translational velocity of $v_t \approx 63$ m/s. In the zipped region, a chain of water molecules resides inside the turning line of the zipped ribbon. This region can be used like an artificial channel, similarly like CNTs.

We have also observed that the folding dynamics can be in some cases influenced by the initial position of the droplet on the graphene ribbon. This is particularly true if the ribbon is significantly wider than the droplet. Then, if the droplet is, for example, placed at the ribbon corner, the system can get to either the zipping or sliding phases. On the other hand, only the zipping phase is observed when the droplet is placed more toward the center of the ribbon edge. These examples
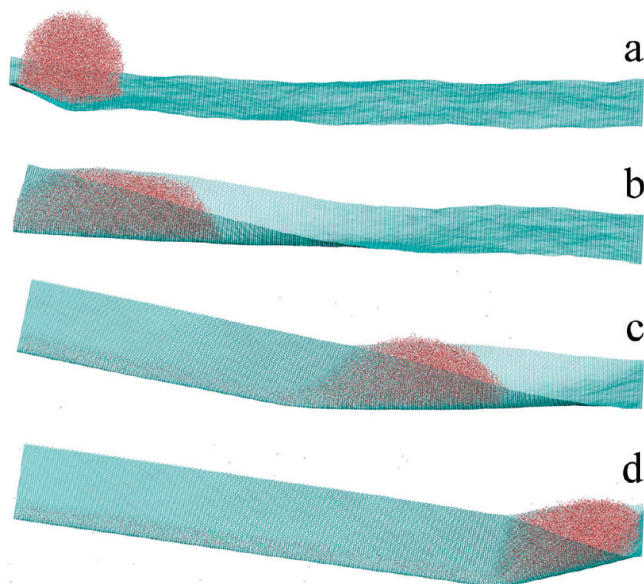
Figure 6. Folding and zipping of a graphene ribbon with the size of 60×16 nm, which is activated and guided by a nanodroplet with $N_w = 17000$ water molecules and the radius of $R_d \approx 5$ nm. (a, b) The ribbon end folds around the droplet. (c, d) The zipping propagates along the ribbon until the fixed end, while water channel is formed in the graphene sleeve.
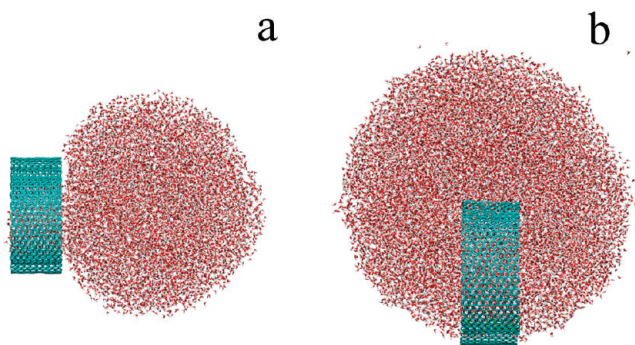

Figure 7. Binding modes of graphene rings based on a ribbon with the size of 30×2 nm, inside water droplets. (a) The stable "capping" configuration of a hydrophobic ring with $N_w = 10000$ waters. (b) The metastable "locking" configuration of a hydrophilic ring with $N_w = 18000$ waters.

show the rich possibilities for droplet controlled folding of graphene systems.

Finally, we briefly characterize coupling of the graphene ribbon ring, shown in Figure 4, to larger droplets, which might have potential applications. Here, we consider cases with a hydrophobic ring, solely made of a graphene nanoribbon of 30×2 nm^2, and a hydrophilic ring, where we replace a flake of 1×2 nm^2 at the tip of the 30×2 nm^2 graphene ribbon by a boron nitride (BN) ribbon.[40] As show in Figure 7, (a) the hydrophobic ring is stable in a "capping" configuration, where it sits on the droplet with $N_w = 10000$ at $T = 300$ K. (b) The hydrophilic ring, with a BN region folded inside, can have a metastable "locking" configuration, in addition to the stable capping configuration on the droplet surface with $N_w = 18000$ (not shown but similar to (a)). In

the locking configuration, the hydrophilic ring is pierced inside the droplet and partly exposes its external surface outside the droplet.

In summary, we have demonstrated that water nanodroplets can activate and guide folding of graphene nanostructures. The folding can be realized by different types of motions, such as bending, sliding, rolling, or zipping that lead to stable or metastable structures, such as sandwiches, capsules, knots, and rings. These structures can be the building blocks of functional nanodevices, with unique mechanical, electrical, or optical properties.[49]

Note Added after ASAP Publication: There was an error in the k_{bond} unit in the Folding of Flakes section in the version published ASAP October 23, 2009; the correct version published ASAP October 27, 2009.

Supporting Information Available: Movies showing nanodroplet-assisted folding. This material is available free of charge via the Internet at http://pubs.acs.org.

References

(1) Shimomura, M.; Sawadaishi, T. *Curr. Opin. Colloid Interface Sci.* **2001**, *6*, 11–16.
(2) Whitesides, G. M. *Small* **2005**, *1*, 172–179.
(3) Addadi, L.; Weiner, S. *Nature* **2001**, *411*, 753–755.
(4) Nam, K. T.; Kim, D. W.; Yoo, P. J.; Chiang, C. Y.; Meethong, N.; Hammond, P. T.; Chiang, Y. M.; Belcher, A. M. *Science* **2006**, *312*, 885–888.
(5) Talapin, D. V.; Shevchenko, E.; Murray, C. B.; Titov, A.; Král, P. *Nano Lett.* **2007**, *7*, 1213–1219.
(6) Shevchenko, E. V.; Talapin, D. V.; Kotov, N. A.; O'Brien, S.; Murray, C. B. *Nature* **2006**, *439*, 55–59.
(7) Bigioni, T. P.; Lin, X. M.; Nguyen, T. T.; Corwin, E. I.; Witten, T. A.; Jaeger, H. M. *Nat. Mater.* **2006**, *5*, 265–270.
(8) Kalsin, A. M.; Fialkowski, M.; Paszewski, M.; Smoukov, S. K.; Bishop, K. J. M.; Grzybowski, B. A. *Science* **2006**, *312*, 420–424.
(9) DeVries, G. A.; Brunnbauer, M.; Hu, Y.; Jackson, A. M.; Long, B.; Neltner, B. T.; Uzun, O.; Wunsch, B. H.; Stellacci, F. *Science* **2007**, *315*, 358–361.
(10) Li, S. L.; Alivisatos, A. P. *Adv. Mater.* **2003**, *15*, 408–411.
(11) Titov, A.; Král, P. *Nano Lett.* **2008**, *8*, 3605–3612.
(12) Novoselov, K. S.; Geim, A. K.; Morozov, S. V.; Jiang, D.; Zhang, Y.; Dubonos, S. V.; Grigorieva, I. V.; Firsov, A. A. *Science* **2004**, *306*, 666–669.
(13) Geim, A. K.; Novoselov, K. S. *Nat. Mater.* **2007**, *6*, 183–191.
(14) Berner, S.; Corso, M.; Widmer, R.; Groening, O.; Laskowski, R.; Blaha, P.; Schwarz, K.; Goriachko, A.; Over, H.; Gsell, S.; Schreck, M.; Sachdev, H.; Greber, T.; Osterwalder, J. *Angew. Chem., Int. Ed.* **2007**, *46*, 5115–5119.
(15) Laskowski, R.; Blaha, P.; Gallauner, T.; Schwarz, K. *Phys. Rev. Lett.* **2007**, *98*, 106802.
(16) Li, X.; Wang, X.; Zhang, L.; Lee, S.; Dai, H. *Science* **2008**, *319*, 1229–1232.
(17) Jiao, L.; Zhang, L.; Wang, X.; Diankov, G.; Dai, H. *Nature* **2009**, *458*, 877–880.
(18) Kosynkin, D. V.; Higginbotham, A. L.; Sinitskii, A.; Lomeda, J. R.; Dimiev, A.; B. K; Price, B. K.; Tour, J. M. *Nature* **2009**, *458*, 872–876.
(19) Tapasztó, L.; Dobrik, G.; Lambin, P.; Biró, L. P. *Nat. Nanotechnol.* **2008**, *3*, 397–401.
(20) Stampfer, C.; Guttinger, J.; Hellmuller, S.; Molitor, F.; Ensslin, K.; Ihn, T. *Phys. Rev. Lett.* **2009**, *102*, 056403.
(21) Ci, L.; Xu, Z.; Wang, L.; Gao, W.; Ding, F.; Kelly, K. F.; Yakobson, B. I.; Ajayan, P. M. *Nano Res.* **2008**, *1*, 116–122.
(22) Campos, L. C.; Manfrinato, R. V.; Sanchez-Yamagishi, J. D.; Kong, J.; Jarillo-Herrero, P. *Nano Lett.* **2009**, *9*, 2600–2604.

(23) Zhu, Z. P.; Su, D. S.; Weinberg, G.; Schlogl, R. *Nano Lett.* **2004**, *4*, 2255–2259.

(24) Jin, W.; Fukushima, T.; Niki, M.; Kosaka, A.; Ishii, N.; Aida, T. *Proc. Natl. Acad. Sci. U.S.A.* **2005**, *102*, 10801–10806.

(25) Chen, Q.; Chen, T.; Pan, G.-B.; Yan, H.-J.; Song, W.-G.; Wan, L.-J.; Li, Z.-T.; Wang, Z.-H.; Shang, B.; Yuan, L.-F.; Yang, J.-L. *Proc. Natl. Acad. Sci. U.S.A.* **2008**, *105*, 16849–16854.

(26) Lee, C.; Wei, X.; Kysar, J. W.; Hone, J. *Science* **2008**, *321*, 385–388.

(27) Bunch, J. S.; Verbridge, S. S.; Alden, J. S.; van der Zande, A. M.; Parpia, J. M.; Craighead, H. G.; McEuen, P. L. *Nano Lett.* **2008**, *8*, 2458–2462.

(28) Gómez-Navarro, C.; Burghard, M.; Kern, K. *Nano Lett.* **2008**, *8*, 2045–2049.

(29) Viculis, L. M.; Mack, J. J.; Kaner, R. B. *Science* **2003**, *299*, 1361.

(30) Braga, S. F.; Coluci, V. R.; Legoas, S. B.; Giro, R.; Galvao, D. S.; Baughman, R. H. *Nano Lett.* **2004**, *4*, 881–884.

(31) Yu, D.; Liu, F. *Nano Lett.* **2007**, *7*, 3046–3050.

(32) Sidorov, A.; Mudd, D.; Sumanasekera, G; Ouseph, P. J.; Jayanthi, C. S.; Wu, S.-Y. *Nanotechnology* **2009**, *20*, 055611.

(33) Wang, B.; Král, P. *Phys. Rev. Let.* **2008**, *101*, 046103.

(34) Martel, R.; Shea, R. H.; Avouris, P. *J. Phys. Chem. B* **1999**, *103*, 7551–7556.

(35) Huang, J.; Juszkiewicz, M.; de Jeu, W. H.; Cerda, E.; Emrick, T.; Menon, N.; Russell, T. P. *Science* **2007**, *317*, 650–653.

(36) Py, C.; Reverdy, P.; Doppler, L.; Bico, J.; Roman, B.; Baroud, C. N. *Phys. Rev. Lett.* **2007**, *98*, 156103.

(37) Ellis, R. J.; Vandervies, S. M. *Annu. Rev. Biochem.* **1991**, *60*, 321–347.

(38) Phillips, J. C.; Braun, R.; Wang, W.; Gumbart, J.; Tajkhorshid, E.; Villa, E.; Chipot, C.; Skeel, R. D.; Kale, L.; Schulten, K. *J. Comput. Chem.* **2005**, *26*, 1781–1802.

(39) MacKerell, A. D., Jr.; Bashford, D.; Bellott, M.; Dunbrack, R. L., Jr.; Evanseck, J. D.; Field, M. J.; Fischer, S.; Gao, J.; Guo, H.; Ha, S.; Joseph-McCarthy, D.; Kuchnir, L.; Kuczera, K.; Lau, F. T. K.; Mattos, C.; Michnick, S.; Ngo, T.; Nguyen, D. T.; Prodhom, B.; Reiher, W. E., III; Roux, B.; Schlenkrich, M.; Smith, J. C.; Stote, R.; Straub, J.; Watanabe, M.; Wirkiewicz-Kuczera, J.; Yin, D.; Karplus, M. *J. Phys. Chem. B* **1998**, *102*, 3586–3617.

(40) In the MD simulations, we apply the Langevin dynamics with 0.01 ps^{-1} damping coefficient, to minimize the unphysical loss of momentum,[33] and the time step is 1 fs. The systems are simulated as NVT ensembles inside periodic cells of the following sizes: Figure 1 (55 × 35 × 35 nm^3), Figure 2 (up) (30 × 35 × 35 nm^3), Figure 2 (bottom) (30 × 35 × 35 nm^3), Figure 3 (15 × 85 × 25 nm^3), Figure 4 (20 × 120 × 20 nm^3), Figure 6 (20 × 75 × 20 nm^3), and Figure 7 (60 × 85 × 60 nm^3). The BN sheet, shown in Figure 7, have charges of e and− e on the boron and nitrogen atoms, respectively.[33] The graphene− water (or graphene−graphene) binding energies are calculated as the difference of the total vdW energy of the system, when the system components are at the normal binding distance and when they are separated by 5 nm. Averaging of the energies is done over 100 consecutive frames of the simulation trajectory, with a 1 ps time interval.

(41) Juniper, B. E.; Robins, R. J.; Joel, D. M. *The carnivorous plants*; Academic Press: San Diego, CA, 1989; ISBN 0-1239-2170-8 .

(42) Lee, K. B.; Park, S. J.; Mirkin, C. A.; Smith, J. C.; Mrksich, M. *Science* **2002**, *295*, 1702–1705.

(43) Duwez, A.-S.; Cuenot, S.; Jérome, C.; Gabriel, S.; Jérome, R.; Rapino, S.; Zerbetto, F. *Nat. Nanotechnol.* **2006**, *1*, 122–125.

(44) Tersoff, J. *Phys. Rev. B* **1992**, *46*, 15546–15549.

(45) Kudin, K. N.; Scuseria, E. G. *Phys. Rev. B* **2001**, *64*, 235406–234515.

(46) Arroyo, M.; Belytschko, T. *Phys. Rev. B* **2004**, *69*, 115415–115425.

(47) Lu, Q.; Arroyo, M.; Huang, R. *J. Phys. D: Appl. Phys.* **2009**, *42*, 102002–102007.

(48) Walther, J. H.; Werder, T.; Jaffe, R. L.; Gonnet, P.; Bergdorf, M.; Zimmerli, U.; Koumoutsakos, P. *Phys. Chem. Chem. Phys.* **2004**, *6*, 1988–1995.

(49) Baughman, R. H.; Cui, C. X.; Zakhidov, A. A.; Iqbal, Z.; Barisci, J. N.; Spinks, G. M.; Wallace, G. G.; Mazzoldi, A.; De Rossi, D.; Rinzler, A. G.; Jaschinski, O.; Roth, S.; Kertesz, M. *Science* **1999**, *284*, 1340–1344.